Observation of seasonal asymmetry in the Range spread F occurrence at different longitudes during low and moderate solar activity

Abimbola O Afolayan[1], Mandeep Singh Jit Singh[1,2], Mardina Abdullah[1,2], Suhaila M Buhari[2,3], Tatsuhiro Yokoyama[4], and Pornchai Supnithi[5]

[1]Center of Advanced Electronic and Communication Engineering, Universiti Kebangsaan Malaysia, 43600 Bangi, Selangor, Malaysia.
[2]Space Science Centre (ANGKASA), Institute of Climate Change, Universiti Kebangsaan Malaysia, 43600 Bangi, Selangor, Malaysia.
[3]Geomatic Innovation Research Group, Faculty of Science, Universiti Teknologi Malaysia, 81310 Johor Bahru, Johor, Malaysia.
[4]Research Institute for Sustainable Humanosphere, Kyoto University, Uji, Japan.
[5]Faculty of Engineering King Mongkut's Institute of Technology Ladkrabang, Bangkok, Thailand

Correspondence: Mandeep J. Singh (mandeep@ukm.edu.my)

Abstract. A comparative study of the equatorial spread F occurrence was conducted at different longitudes during 2010 and 2013 representing the low (LSA) and moderate (MSA) solar activity periods respectively. The ionogram data were recorded at low latitude stations including Jicamarca (JIC;75.76° W,8.17 ° S); Fortaleza (FZA; 38.52 ° W, 3.73 ° S); Ilorin (ILR; 7.55 ° E,9.93 ° N); Chumphon (CPN; 88.46 ° E, 11° N)and Kwajalein (KWA; 167.73 ° E, 8.72° N).The range type spread F (RSF) occurrence was manually recorded at an hour interval between 18:00 – 06:00 LT and a monthly average of the RSF occurrence was estimated for each season. The longitudinal distribution of the RSF occurrence features included the observed difference in the onset time, duration and seasonal occurrence peak. The seasonal asymmetry in the RSF occurrence distribution was analyzed in relation to the zonal drift reversal's effect on the plasma irregularity initiation. We believe that the inconsistent equinoctial asymmetry pattern in the RSF occurrence is modulated by the seasonal/longitudinal variation of the zonal drift reversal delay during both solar epochs. Likewise, the seeding effect and the background ionospheric condition were also considered as major factors influencing the frequency of irregularity generation in these regions.

1   Introduction

The equatorial spread F (ESF) is a night time phenomenon that describes the observed ionospheric F layer electron density irregularity within the equatorial or low latitude region and it is usually depicted as the widespread of the echo trace on the ionogram measurement (Booker and Wells, 1938; Bowman, 1990).This echo spread along the frequency band or height range is due to the scattered signal reflection from the multiple paths caused by the irregular ionospheric plasma density profile. The scale size of these plasma irregularities ranges between a few centimeters and hundreds of kilometer (Basu et al., 1978; De Paula et al., 2010). The ESF is usually initiated after the local sunset due to the rapid rise of the F layer and this generates a steep

bottom-side plasma density gradient as a result of the abrupt reduction of the E region ionization level. The Raleigh-Taylor (R-T) instability excited in the bottom-side is considered as the mechanism responsible for the initiation and non-linear growth of the plasma depletion (Woodman and La Hoz, 1976). The vertical plasma drift near the local post-sunset driven by the pre-reversal enhancement (PRE) of the zonal electric field is recognized as the major factor controlling the ESF morphology across the different seasons and longitudes (Abdu, 2001; Dabas et al., 2003; Lee et al., 2005). The PRE rapidly elevates the ionosphere into a higher altitude region, where the collision frequency is lower and more conducive for further plasma depletion growth by the R-T instability mechanism (Fejer et al., 1999; Woodman and La Hoz, 1976). Though, recent studies (Candido et al., 2011; Narayanan et al., 2014; Stoneback et al., 2011) have also analyzed the probable role of several other parameters involved in the plasma irregularity initiation over the period characterized by weak background ionospheric condition. Observation of large ESF occurrence rate during the low solar activity has been attributed to the modulation of the post-sunset electrodynamics by the gravity wave (GW) induced perturbation electric field (Abdu et al., 2009; Aveiro et al., 2009). While the neutral wind intensity and direction is a dominant factor in the observed post-midnight ESF occurrence pattern (Dao et al., 2017; Sastri et al., 1994).

The plasma irregularity occurrence around the equatorial/low latitude region often distorts the L-band signal, thereby causing poor performance of the communication or navigation systems such as the Global Positioning System (GPS) (Aarons et al., 1997; Jiao and Morton, 2015). Therefore, it is important to understand the role of the different precursory factors influencing the spread F morphology under varying ionospheric conditions. This complex phenomenon has been explored widely by past studies (Su et al., 2009; Tsunoda, 2010a; Vichare and Richmond, 2005) and there are presently deliberate efforts to improve the prediction accuracy of spread F occurrence distribution pattern across the different regions.

The complex interaction between the E and F region dynamo system in the presence of conductivities and the magnetic field are responsible for the different electrodynamic phenomenon at the low latitude region (Haldoupis et al., 2003; Miller, 1997). During the daytime, the F region divergent current causes an accumulation of the downward polarization electric field at the bottom-side of the region. On the other hand, the E region polarized electric field concurrently drives a closure current mapped along the magnetic field line into the F region that diminishes the F region vertical current (Abdu et al., 1981; Eccles et al., 2015; Heelis, 2004). The field line integrated Pedersen conductivity shorts out the F region dynamo electric field and significantly reduces the zonal plasma drift due to the high E region conductance during the daytime. However, the decay and the consequent reduction of the E region conductance during the nighttime causes a significant increase in the field-aligned Pedersen conductivity ratio. This generates a large vertical current by the F region dynamo and the resulting downward electric field drives the plasma in the direction of the neutral wind. Thus, the F layer dynamo electric field created by the divergence current dominates near the sunset period and this induces the eastward plasma motion in the F region at an ExB velocity. The PRE vertical plasma drift is associated with the enhanced eastward electric field caused by the significant decay of the E region conductivity. This combined with the rapid chemical recombination rate of the E layer around the sunset period results in the increased steepness of the bottom-side plasma density gradient. Hence, the large vertical drift enhances the plasma instability triggered by the seed perturbation and subsequently the R-T instability growth rate. On the other hand, a prolonged eastward equatorial electrojet (EEJ) could cause a reduced field aligned conductivity gradient due to the small vertical current driven by

the post-sunset conjugate E region. Thus, the resulting zonal electric field accumulation at the F layer base can only generate a relatively small PRE vertical drift. This ionospheric electrodynamics effect also yields a zonal drift reversal delay which has also been shown as a strong factor influencing the instability growth rate (Su et al., 2009).The seasonal/longitudinal distribution of the ESF occurrence rate is dependent on the declination angle of the magnetic field. The longitudinal gradient of the field-aligned Pedersen conductivity becomes steepest when the sunset terminator is well aligned with the local magnetic flux tube, thereby resulting in a simultaneous relative sunset time at the magnetic conjugate E regions that are coupled to the F region (Abdu et al., 1992; Maruyama and Matuura, 1984; Tsunoda, 1985; Tsunoda et al., 2015). Hence, the PRE of the eastward electric field is maximum at such longitude and likewise the elevation of the F layer altitude near sunset. The base of the F region gets lifted to greater heights making it conducive for the plasma instability growth. Therefore, the longitudinal variation in the seasonal distribution of the ESF occurrence rate is associated with the variation of the solar terminator-magnetic field alignment (STBA) and their distinct local sunset time equatorial electric field system. Due to the near-zero sunset time lag between the conjugate E regions during the equinox period, there is usually a good alignment. On the other hand, the solstice months have been shown in several studies (Hoang et al., 2010; Su et al., 2008) to have good (bad) alignments during June solstice (December solstice) at longitudes of positive (negative) magnetic declination. The seasonal/longitudinal distribution of the equatorial plasma irregularity has been extensively reported to be strongly correlated with the seasonal variation of the STBA (Abdu et al., 1981; Li et al., 2008; Su et al., 2008). However, a recent study described the significant ESF occurrence during the solstice seasons at the West African and Central Pacific region to be inconsistent with the defined theory of the declination angle influence on the spread F longitudinal distribution (Tsunoda et al., 2015). These discrepancies are considered noteworthy for an improved understanding of the features of global plasma irregularity distribution as influenced by different background atmospheric conditions.

This study is mainly focused on examining the salient features of the spread F local time distribution patterns at these longitude sectors during the equinox and solstice seasons of the low (2010: 80sfu) and moderate (2013: 122.7sfu) solar activity period. Furthermore, the role of the zonal drift reversal time was investigated in relation to the observed asymmetry during the equinox and solstice seasons. Though the asymmetry pattern during the equinoxes is yet to be well defined and it varies across the longitudes during both solar epochs. This analysis tended to understand the major phenomenon responsible for the equinoctial asymmetry of the ESF occurrence at each region. Thus, the probable competing role of the vertical plasma drift, virtual height and the seed perturbation were considered in the analysis of the observed spread F distribution at these longitude sectors.

2   Data and methods

The ESF events were recorded at the equatorial stations situated at different longitudes (Jicamarca (JIC) station, Peru; Fortaleza (FZA) station, Brazil; Ilorin (ILR) station, Nigeria; Chumphon (CPN) station, Thailand and Kwajalein (KWJ) station, Marshal Island), as shown in Table 1. The table lists the geographic coordinates and the sunset time at each of the stations selected for the study of the spread F irregularity distribution. These are stations within the Southeast Asia low-latitude ionospheric network (SEALION) and Global Ionospheric Radio Observatory (GIRO) network as indicated in Fig. 1. The observation data

were taken using the digital ionosonde (DP-S 4 digisonde) and analogue type FMCW (frequency modulated continuous wave) (Maruyama et al., 2008; Reinisch and Galkin, 2011). Since the ESF events are very rare during the daytime, our investigation was limited to the time interval between 18:00 – 06:00 LT. The ionograms were examined at an hour interval for the presence of range spread F (RSF) or strong range spread F (SSF). Subsequently, the monthly mean of the RSF occurrence percentage variation over the defined local time interval was then estimated using the relation:

$$hourly occurrence\% = \frac{(number\, of\, ionograms\, in\, each\, hour\, with\, RSF)}{(total\, number\, of\, ionograms\, in\, an\, hour\, for\, that\, month)} \times 100 \tag{1}$$

Only the quiet days ($\Sigma\kappa\rho \leq 24$) were considered for each month representing the different seasons during the low (F107A <100 sfu) and moderate (F107A <150 sfu) solar activity period (Wang et al., 2017). The seasonal variation of the ESF events was analyzed according to the available data at each of the ionosonde stations listed in Table 1. Thus, the data taken from March, June, September and December months of 2010 (2013) represents the March equinox, June solstice, September equinox and December solstice of LSA (MSA) respectively.

Table 1. Description of the stations' geographic location and their local sunset time range.

Station	Longitude (degree)	Latitude (degree)	Dip Lat.	Declination angle	Sunset time (LT)
Jicamarca (JIC)	-75.76	-8.17	3.75	-3.24	18:45 – 19:15
Fortaleza (FZA)	-38.52	-3.73	-6.89	-20.11	18:30 – 18:45
Ilorin (ILR)	4.5	8.53	-4.27	-1.69	18:00 – 19:00
Chumphon (CPN)	99.37	11	3.76	-1.46	19:30 – 20:15
Kwajalein (KWJ)	167.73	8.72	3.62	7.62	19:30 – 20:15
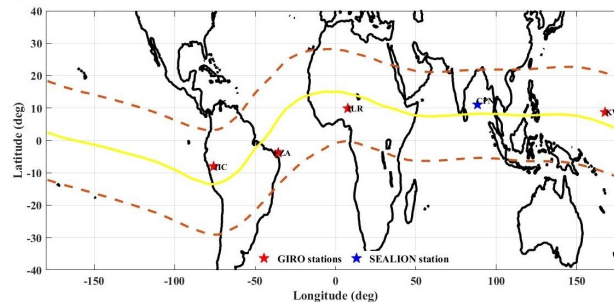
Figure 1. The geographic location of the ionosonde stations and their corresponding observatory network shown by the red (GIRO) or blue (SEALION) marker

The recorded ionogram signatures are usually divided into frequency spread F (FSF), mixed spread F (MSF), range spread F (RSF) and strong range spread F (SSF) (Shi et al., 2011). However, this study considers only the RSF and SSF type during the observation of the plasma irregularity events recorded by the ionograms across these longitudes. The RSF signature represents the instance of the ordinary F layer trace spreading mainly along the altitude as shown in Figure 2, and the SSF which is de-

105 scribed as a type of RSF has its ordinary trace extending significantly beyond the local foF2 (Bowman, G. G., 1960; Bowman, 1998). Hereafter, we will refer to the March, June, September and December seasons as M-equinox, J-solstice, S-equinox and D-solstice respectively.
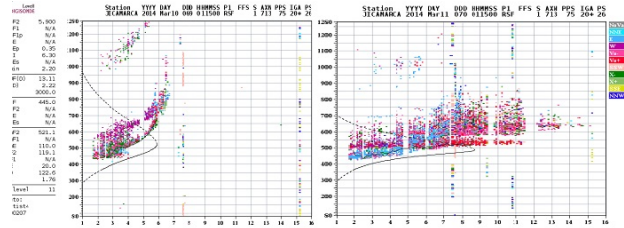
Figure 2. Sample of the RSF (left) and SSF (right) recorded using the DPS-4 digisonde at the Jicamarca station

The monthly average of the scaled virtual height was taken as a representation of the seasonal variation of the near sunset

110 vertical plasma drift recorded at each of the ionosonde stations. The seasonal variation of the virtual height taken during the low solar activity (LSA) and moderate solar activity (MSA) period was then analyzed in correspondence to the RSF occurrence distribution. Based on data availability across the considered stations as shown in Figure 3, the data taken during the year of 2010 represents the LSA period while the year of 2013 represents the MSA period.
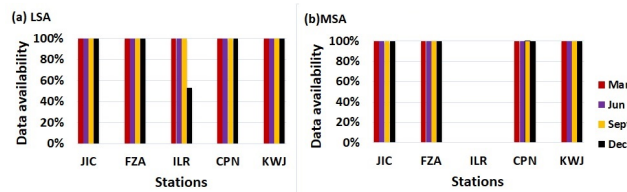
Figure 3. The ionogram data availability at the Jicamarca, Fortaleza, Ilorin, Chumphon and Kwajalein stations during the (a) LSA and (b) MSA period

3 Results

115 Figures 4 and 5 present the hourly distribution of the RSF occurrence percentage across the different longitudes during the LSA period and the MSA period, which was averaged over each month based on the available data at these stations. The

monthly mean RSF occurrence percentage was higher at all the considered longitudes during the equinox months than the solstice months of the LSA year. The percentage of RSF occurrence percentage and duration is highest at the ILR station for all the seasons, while the minimum monthly mean RSF occurrence percentage was recorded at the KWJ station. Generally, the average duration of the post-sunset plasma irregularity in Fig. 4. varies across these longitude sectors, while the starting time of the spread F during the equinox and D-solstice months varies mostly between 18:00 and 20:00 LT. The observed onset time variation of the RSF occurrence corresponds with the varying sunset time across the different longitudes as shown in Table 1, except cases with significant delay. Figure 4 shows that the maximum RSF occurrence percentage was mostly observed before the midnight period (around 21:00 LT) during most seasons at each longitude. However, there are months which have a significantly larger RSF occurrence percentage near midnight than at 21:00 LT. This could be attributed to either the irregularity onset delayed till pre-midnight period as a result of the ionospheric condition or multiple days with irregularities drifting from a distant location into the ionogram's field of view (Balan et al., 2018; Narayanan et al., 2014).

Another important observation was the large RSF occurrence percentage of $\sim$ 70% at ILR but relatively smaller occurrence rate of $\sim$ 30% at KWJ during the J-solstice of the LSA year. While the RSF occurrence percentage was below 10 % at the other longitude regions. The large RSF occurrence percentage recorded at the ILR stations was contrary to the expected longitudinal distribution based on the defined low and high ESF longitude range during the J-solstice (Su et al., 2007). Likewise, the other relevant observations across the different longitudes during the J-solstice, such as the significantly delayed irregularity onset at KWJ will be further discussed in a later section.
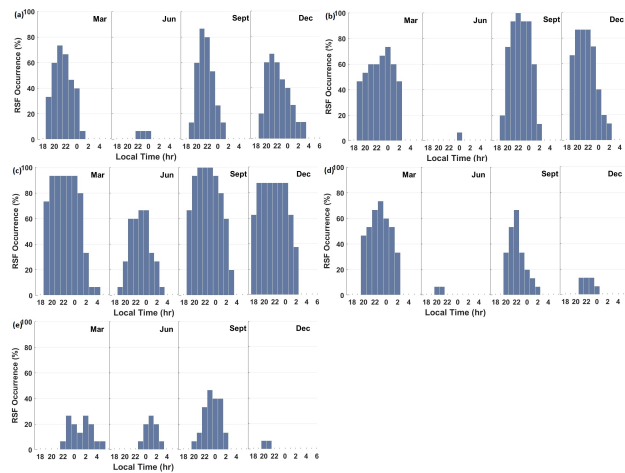
Figure 4. Occurrence rate of RSF during LSA period at the (a) Jicamarca (b) Fortaleza (c) Ilorin (d) Chumphon and (e) Kwajalein stations

Figure 5 shows that there was above 30 % increase in the RSF occurrence percentage across all the stations during the M-equinox of the MSA period. The spread F equinox asymmetry was very visible in all the regions except at the FZA station, where the hourly peak of the RSF occurrence percentage was approximately equal at both equinox seasons. Unlike the

equinoctial asymmetry, during the LSA which showed an inconsistent longitudinal variation the M-equinox has a significantly larger RSF occurrence percentage at the CPN, JIC and KWJ stations during the MSA. On the other hand, Fig. 4 and 5 show a similar solstice asymmetry in the observed RSF occurrence percentage during both solar epochs. The RSF occurrence percentage during the J-solstice of the MSA period was less than or $\sim 10\%$ at all the stations except at the KWJ station.. There was $\sim 30\%$ increase in the RSF occurrence percentage at the KWJ station during J-solstice and the irregularity onset time was also much earlier (immediately after the local sunset) than the LSA onset time. Su et al., (2009) have already established a relationship between the zonal drift reversal time and the velocity drift amplitude, instability growth rate and irregularity onset in the $150° - 170°$ longitude range. Hence, the delayed onset and the relatively small RSF occurrence percentage at this region during the LSA will later be discussed further in relation to the zonal drift reversal effect and the weak background ionospheric condition in the region.

The negative declination angle region was described as the high ESF longitude during the D-solstice due to the strong magnetic flux tube-solar terminator alignment (Tsunoda, 1985). Furthermore, the large declination angle in the Brazilian region causes a relatively simultaneous local sunset at the conjugate E region and thereby driving a stronger eastward polarization electric field at the equatorial F region (Abdu et al., 1981; Tsunoda, 2010a.Correspondingly the highest RSF occurrence percentage peak was recorded at the FZA station for both the LSA ($\sim 85\%$) and MSA ($\sim 100\%$) period. The pre-midnight RSF occurrence percentage peak recorded $\sim 15\%$ increase at the FZA and CPN stations during the D-solstice, while there was no RSF occurrence at the KWJ station during the MSA period. The reduced RSF occurrence percentage at KWJ during D-solstice correlates with the described anti-solar spread F occurrence pattern at the low ESF longitudes during the solstices (Su et al., 2007).
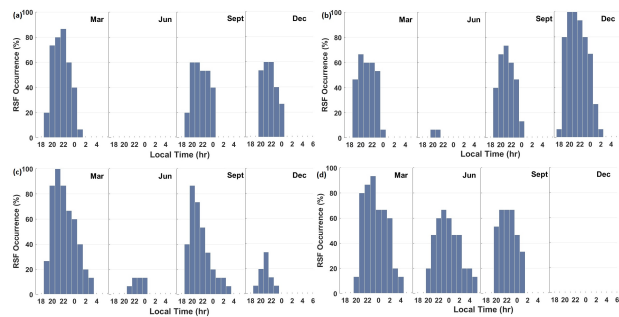
Figure 5. Occurrence rate of RSF during the MSA period at the (a) Jicamarca (b) Fortaleza (c) Chumphon and (d) Kwajalein stations

Figures 6(a-d) show a comparison between the RSF occurrence percentage during the MSA and LSA at each of the four stations with sufficient data. There was a significant difference between the spread F occurrence percentage during the LSA and MSA period across all seasons at most of the stations except at the JIC and FZA stations. The RSF occurrence percentage at both stations varies inversely with the solar flux index during S-equinox, while the approximately equal percentage was recorded during the D-solstice of both solar epochs. The observed negative solar flux dependence pattern at these longitudes

during the S-equinox could be attributed to the growing effect of the density scale length on the irregularity growth during this season as the solar flux increases. Hence, the S-equinox and D-solstice seasons were described as having a more conducive ionospheric condition for the generation of RSF at this longitude region during LSA.

165 There was an absence of RSF occurrence at the JIC station during J-solstice of the MSA. The inverse correlation between the solar flux intensity and the RSF occurrence have been observed at the low ESF longitudes from $230° − 10°$ and $90° − 260°$ during the J-solstice and D-solstice respectively (Su et al., 2007)and attributed to the neutral wind effect. Their result was corroborated by the diverging neutral meridional wind pattern observed during the J-solstice at this longitude and the expected effect of the increased meridional wind on the irregularity growth suppression during the MSA. The peak RSF occurrence

170 percentage at most of the longitudes during the LSA is usually around the midnight period while the peak is closer to the local sunset time during MSA. However, through observation of the RSF occurrence features as shown in Fig. 6(a-b) indicated that the near sunset peak and the rapid increase of the RSF occurrence percentage were more consistent for the seasons with an expectedly significant post-sunset rise (PSSR). The typical plasma irregularities formed around the sunset period are dominated by the PRE dynamics, while some other mechanisms may play a substantial role in the generation of the post-midnight ESF

175 events (Dao et al., 2017; Otsuka, 2018).
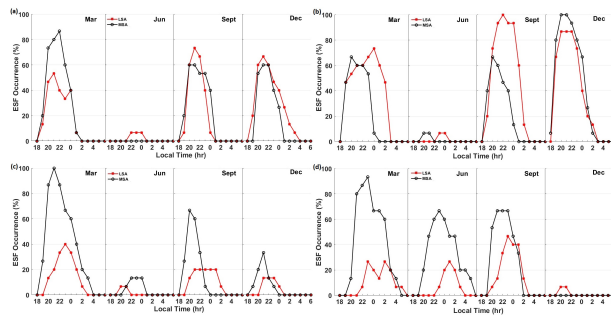
Figure 6. The percentage of ESF occurrence during the LSA and MSA period for (a) Jicamarca (b) Fortaleza (c) Chumphon and (d) Kwajalein stations

Figures 7(a-b) show the local time variation of the monthly mean virtual height ($h\prime F$) during the LSA and MSA period across the five longitude regions considered in this study. Likewise, the corresponding annual variation of the sunset time lag was also presented in Fig. 7(c). This represents the difference between the local sunset times at the foot-points of the conjugate E region that connects with the F layer base. The longitudinal variation pattern of the PSSR is consistent with the earlier numer-

180 ical simulation by Vichare and Richmond, (2005), which observed that the longitudinal PRE variation have its peak between $290°$ E and $30°$ E longitude region. The observed PSSR of the $h\prime F$ (representing the pre-reversal enhancement (PRE) of the vertical plasma drift near the local sunset) is generally higher during the equinoctial and D-solstice months of MSA than the corresponding seasons of the LSA period. In the case of J-solstice months, the near sunset enhancement of the vertical plasma drift as shown in Figure 7(a-b) was almost absent during both solar epochs. Though based on the comparison with the annual

sunset time lag variation for each of the regions as shown in Fig. 7(c) , the PRE magnitude was expected to be larger at the KWJ station than the other regions. However, the relatively large magnetic field strength in the Asian (CPN) and Central Pacific (KWJ) region (Su et al., 2009; Vichare and Richmond, 2005) causes the weak PRE mostly observed in this regions during both solar epochs. Such zonal variation of the factors including the eastward electric field, field-aligned Pedersen conductivity and magnetic field strength contributes to the resultant zonal variation of the vertical plasma amplitude (Abdu, 2016; Vichare and Richmond, 2005).

The sunset time lag was inconsistent with the observed solstice asymmetry in the PSSR at the low declination angle regions. The equatorial electrojet (EEJ) has been identified as a likely controlling factor in the seasonal variation of the near local sunset PSSR (Abdu et al., 1981). The effect of the post-sunset EEJ presence result from the strong dependence of the PSSR on the longitudinal gradient of the Pedersen conductivity. Hence, a seasonal modulation of the EEJ strength by tidal winds from the lower atmosphere will contribute to the PRE. Apart from slow decay of EEJ due to the prolonged sunset duration between the conjugate E regions, the seasonal ionospheric density variation could also influence the field-aligned current and the changes in the zonal drift reversal. Su et al., (2009) highlighted the influence of the prolonged eastward EEJ on the zonal drift reversal during J-solstice, which is expectedly accompanied by a weak vertical plasma drift in the F region. On the other hand, an equinoctial asymmetry in the PSSR was also prominent during the MSA at all the regions except the KWJ station, where the weak E/B generally reduces the post-sunset PRE vertical drift. The asymmetry is mainly attributed to the increasing difference between the neutral density components at both equinoxes as the solar flux increases (Manju and Madhav Haridas, 2015).
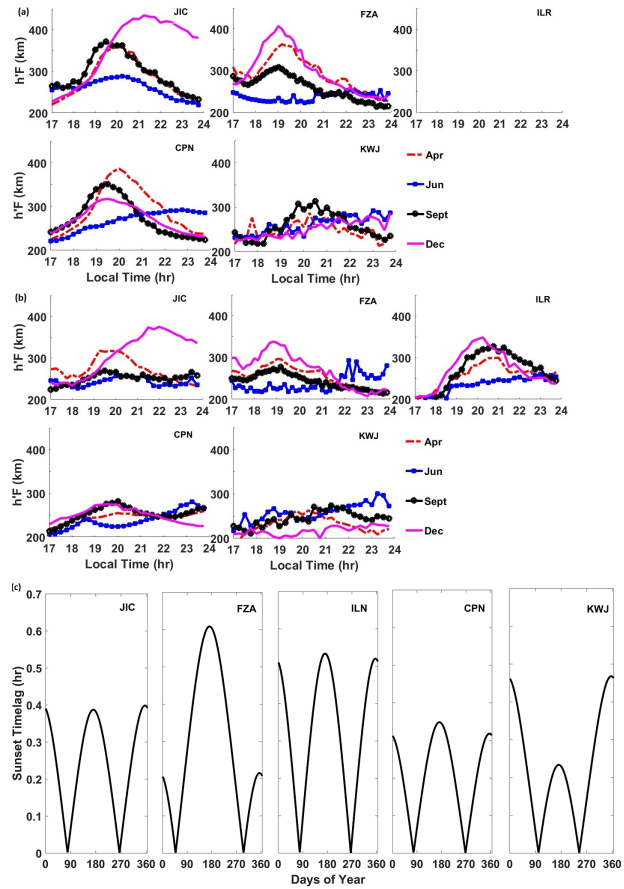
Figure 7. Monthly average of the virtual height during (a) MSA, (b) LSA and (c) The estimated sunset time lag between the geomagnetic conjugate points for each of the longitude sectors

4 Discussion

The observed longitudinal variation of the spread F occurrence during the different seasons of both solar epoch have shown a strong similarity with the earlier studies (Klinngam et al., 2015; Pezzopane et al., 2013; Pietrella et al., 2017; Su et al., 2007; Tsunoda et al., 2015). These studies have deployed different measurement techniques to establish a strong linear relationship between the eastward electric field enhancement near the sunset and the seasonal/longitudinal distribution of the spread F occurrence across the solar epoch (Fejer et al., 1999; Huang, 2018; Stolle et al., 2008; Whalen, 2002). The PRE of the zonal electric field around the local sunset uplift the F layer into the altitudinal region suitable for the rapid plasma irregularity growth by the $R - T$ instability mechanism. Thus, the vertical drift amplitude was described as the dominant factor influencing the difference in the observed features such as the onset time, occurrence rate or latitudinal extension of the plasma irregularity

across the various season or longitude.

However, other factors such as the zonal drift reversal could also make significant difference in the post-sunset electrodynamics effect on the observed plasma irregularity features across different seasons. For example, the delayed (2 hours lag) RSF onset time during the M-equinox and J-solstice of the LSA compared to the observed characteristics at KWJ during the corresponding seasons of the MSA period shown in Figures 4 and 5. This is attributed to the delayed zonal drift reversal effect on the instability growth rate during the LSA (Su et al., 2009). The eastward reversal of the zonal plasma drift in the upper ionosphere region causes a vertical shear motion and the initiation of the irregularity growth (Kudeki and Bhattacharyya, 1999). Su et al., (2009) presented a theoretical analysis of the zonal drift reversal effect on the post-sunset dynamics at the F region base using the simulation result obtained at the KWJ longitude during the J-solstice season. The zonal drift was expressed as;

$$V_\Phi = -\frac{\sigma_H}{\sigma_P}\frac{E_\Phi}{B} + U_\Phi + \frac{\sigma_H}{\sigma_P}U_p - \frac{J_p}{\sigma_P B} \tag{2}$$

Where σ_P and σ_H represent the Pedersen and Hall conductivities respectively, B is the magnetic field. E, U and J represent the electric field, neutral wind and current respectively, while ¶ and Φ are the components in the vertical and zonal direction. The average F region altitude near local sunset is above 200 km and $\frac{\sigma_H}{\sigma_\rho}$ tends toward nil in this altitude range, hence the first and third term in eq.1 are negligible. The zonal drift reversal delay was described as being strongly influenced and indirectly proportional to the flux tube integrated Pedersen conductivity. Hence, an expectedly denser ionosphere and a corresponding increase in the Pedersen conductivity during the MSA will cause an earlier zonal drift reversal and larger occurrence rate as shown in Figure 5. Likewise, the significant difference between the irregularity onsets at both equinoxes could also be as a result of the seasonal variation of the zonal drift reversal. This assumption is due to the disappearance of the RSF onset time delay at KWJ during M-equinox of the MSA as shown in Figure 5. Though, further investigation might be required to ascertain that the same phenomenon was responsible for the delayed onset time during the M-equinox season of the LSA.

The observed asymmetry in the RSF occurrence percentage equinoxes and solstices at the different longitudes during both solar epochs were shown to be controlled by different mechanisms entirely (Manju and Madhav Haridas, 2015; Tsunoda, 2010b). In the case of the equinox asymmetry, the occurrence percentage is higher during the S-equinox at the JIC, FZA and KWJ stations during the LSA period. While the CPN and the ILR stations show approximately equal occurrence percentage during both equinoctial seasons. The equinox asymmetry is most visible at the Brazilian and Peruvian longitude during the LSA. Figure 7a shows an approximately equal $h'F$ peak at both equinoxes, which is inconsistent with the observed RSF occurrence asymmetry across these longitudes during the LSA.

In contrast, the equinoctial asymmetry of the RSF occurrence during the MSA as shown in Figure 7(b). conforms with the corresponding larger $h'F$ peak during the M-equinox season at these stations. Manju and Madhav Haridas, (2015) explored the probable relationship between the observed equinox asymmetry in the threshold height $(h'F_c)$ the ESF occurrence percentage and the O/N_2 ratio. This asymmetry was shown to have a strong solar flux dependence. They associated that with a significant difference between the expansions of the thermosphere at both equinoxes as the solar flux increases, which expectedly reflects

on the defined $h'F_c$. This relationship between the thermospheric neutral compositions and the post-sunset dynamics of the F region have also been shown by the earlier studies (Batista et al., 1986; Qian et al., 2009).

The neutral density in the upper thermosphere is known to change with a variation in the O/N_2 ratio, and the post-sunset vertical drift was established to have a directly proportional relationship with the neutral density (Batista et al., 1986; Manju and Madhav Haridas, 2015). Thus, the higher O/N_2 ratio during the M-equinox as reported by Manju and Madhav Haridas, (2015) is expected to correspond to a higher vertical drift peak during this period. Figure 7(b). presents a similar pattern in the estimated PSSR during the equinoctial months. The observed difference in the $h'F$ peak is more significant during the MSA, while during the LSA period, the observed PRE peak was approximately equal for both equinoxes across the different regions. From Figure 4, the Brazilian region recorded a large difference between the RSF occurrence percentages during the equinox seasons of the LSA period. The RSF occurrence percentage was larger during the S-equinox season at the KWJ, JIC and FZA stations. This is attributed to the comparably reduced collision frequency effect on the irregularity growth rate due to the lower neutral density at this season. Consequently, the requisite PRE for irregularity occurrence is smaller than the threshold during M-equinox (Manju and Madhav Haridas, 2015). Hence, the threshold height for RSF occurrence in a season would be dependent on the average neutral density during that season.

The decay of the EEJ current is relatively abrupt during equinox at the large declination angle region and the zonal drift reversal is directly related to the zonal wind reversal as described by Eq.1. In the absence of EEJ dependent factor $\frac{J_\rho}{\sigma_\rho\,B}$ in Eq.1 will cause the zonal dirft reversal to occur at almost the same time with the zonal wind and yield a strong background condition for the irregularity growth at both equinoxes. However, the sunset time lag tends to change rapidly at the large declination angle region and fig.7c shows that it reaches almost twice the peak time lag at the small declination angle during the solstice season. As the sunset time lag increases, the short-circuiting effect on the post-sunset F region dynamo persists longer. This implies that the PSSR during the later days of the season will mostly fall below the defined threshold height for RSF occurrence during M-equinox. An unpublished result taken at the FZA station showed that the RSF occurrence percentage reduces from March to April of the same LSA year by $\sim 40\%$ On the other hand, the threshold height during S-equinox is smaller and the rapid change in the sunset time lag would have a lesser effect on the irregularity occurrence rate. Hence, the RSF occurrence percentage will be larger during the S-equinox at these longitude regions as described earlier. Coincidentally, the observed equinoctial asymmetry during the LSA seems to be more prevalent at the stations with the larger declination angle. Madhav Haridas et al., (2015) analyzed the role of the sunset time lag on the vertical drift peak in the Indian longitude region during the equinoxes and showed that the partial short-circuiting effect persists longer during the LSA and MSA period. In the case of the small declination angle regions, we assume that the larger density during the M-equinox will cause a stronger suppression of the EEJ current effect and an earlier zonal drift reversal time. Thus, the seeding of the R-T instability occurs under a very conducive ionospheric condition for optimal instability growth rate than during the S-equinox. The effect of the fourth term in eq.1 on the difference between the zonal drift at the two equinoxes might become more significant as the asymmetry in the neutral density increases during the MSA (Manju and Madhav Haridas, 2015).

The PSSR during the equinoxes shows a comparably similar pattern with the observed equinoctial asymmetry in the RSF occurrence percentage for all the regions during MSA except in the Brazilian region (represented in Fig. 4 and 5). Where

the RSF occurrence percentage peak was approximately equal for both equinox seasons. The American sector has the largest field–aligned Pedersen conductivity and we assume that the significant increase in the conductivity during MSA would nullify the asymmetry in the zonal drift reversal time at this region during equinoxes. On the contrary, this also means a significant increase in the ionospheric density and the threshold height. Hence, the inverse solar activity dependence of the RSF occurrence percentage observed at the JIC and FZA stations during the S-equinox as shown in Fig. 6(a-b) is attributed to an increased density scale length. The observed large RSF occurrence percentage during the S-equinox of the LSA at these longitudes was earlier related to the effect of the contracted ionospheric density. However, the increase in the bottom-side density scale length during the MSA (Lee, 2010) will increase the threshold PRE for the irregularity occurrence (Smith et al., 2016). The inconsistent equinoctial asymmetry pattern at different solar flux index was also observed in the Atlantic region during the study of the global equatorial plasma bubble occurrence (Gentile et al., 2006). Similar inverse solar activity pattern was observed at this longitude region by Su et al., (2007)) as shown in their Fig. 3b but less prominent than our result due to the difference in the altitude of data observation.

During the solstice seasons, the observed asymmetry in the PRE of the F layer and the RSF occurrence percentage at the low declination angle longitudes are inconsistent with the corresponding sunset time lag. Unlike the FZA and KWJ stations where the asymmetry between the solstices could be explained by the difference in the sunset time lag, the other three Ionosonde stations have approximately the same sunset time lag at both solstices. The results showed larger RSF occurrence percentage during the D-solstice at these longitudes. The significant asymmetry in the ionospheric density distribution during the solstice seasons is considered as a probable factor in this case. There is post-sunset EEJ current due to large sunset time lag during the solstice seasons, which strongly affects the instability growth rate. The larger density during D-solstice indicates an earlier zonal drift reversal and a more conducive ionospheric condition for the seeding of the R-T instability process (Su et al., 2009). In a similar discussion, Tsunoda, (2010a) has attributed the observed asymmetry in the RSF occurrence during the solstices to the seasonal variation of the convective gravity wave (GW) sources at these longitudes and proposed the GW phase front and magnetic field line alignment (GWBA) hypothesis. This has been extensively discussed by previous studies (Li et al., 2016; Su et al., 2014; Tsunoda, 2010a) but further analysis is considered necessary to substantiate the correlation between the seasonal distribution of GW and RSF occurrence across these longitudes. However, the presence of a large GW amplitude is widely considered as a requisite condition for the generation of spread F under a weak background ionospheric condition (Abdu et al., 2009; Manju et al., 2016). Therefore, the frequent GW occurrence recorded in the Asian and African regions (Su et al., 2014) and consequently the seeding effect is expected to have played a significant role in the observed plasma irregularity generation in this regions. Apart from the requisite GW and $\vec{B}$ alignment, a large local electron density was described as an important prerequisite for the large ESF growth (Krall et al., 2013). The large electron density is considered necessary to support the GW-induced electric field and the plasma instability growth. Coincidentally, the peak electron density in both regions (unpublished result) shows similar seasonal variation with the RSF occurrence percentage during LSA as shown in fig.4. Though, these plasma irregularities will be confined mostly to the low altitude region, especially in the Asian region. This is due to the strong dependence of the altitudinal/latitudinal growth of irregularity on the PRE strength. The weak PRE at CPN results from the large magnetic field strength and a small field line integrated conductivities at this longitude sector. Under such circumstance,

the GW induced perturbation electric field might be suppressed and reduced impact on the instability growth across these longitudes in spite of the large GW frequency. An analysis based on satellite data would likely observe significantly smaller RSF occurrence percentage in this region during this period. Likewise, Kil and Heelis, (1998) reported that the longitudinal distribution of the ESF occurrence is dependent on the height of observation and the occurrence probability at the low altitude could be related to the seed perturbation from the tropospheric source.

5 Conclusions

The statistical result of the hourly variation of the RSF occurrence percentage across different longitude sectors was investigated during the MSA and LSA period for stations close to the magnetic equator. The manual observation of the seasonal variation of the RSF occurrence pattern using the ionogram data revealed the distinct RSF occurrence features at each of the regions. This highlighted the complex morphology of the ESF events and the diverse role of the different factors contributing to plasma irregularity initiation across the different longitudes during the MSA and LSA. The large RSF occurrence percentage at the West African region (ILR) under the weak ambient ionospheric condition of the LSA period was attributed to the presence of strong GW occurrence in the region. Other important observations included the varying longitudinal pattern of the equinoctial asymmetry during the LSA and MSA. The longitudinal/seasonal variation of the zonal drift reversal time effect on the RSF onset was associated with the observed inconsistency in the asymmetry pattern during the equinoctial season of both solar epochs. Likewise, an anti-solar activity variation of the ESF occurrence percentage was also observed at the JIC and FZA stations during the S-equinox. This was attributed to the possible role of an expected increase in the bottom-side density scale length with the solar flux index. The presented results have shown the significant effect of the zonal drift reversal time on the seeding of a plasma irregularity and consequently the number of irregularity occurrence during a season.

Acknowledgements. The authors thank the several institutions responsible for the ground-based observations and Ionosonde database used in this study. Thanks are also due to D. Okoh and O. Montenbruck who offered meaningful assistance with the estimation of the sunset time lag. The authors are also grateful to the anonymous referees for their suggestions and evaluation of this paper.

References

Aarons, J., Mendillo, M. and Yantosca, R.: GPS phase fluctuations in the equatorial region during sunspot minimum, Radio Sci., 32(4), 1535–1550, doi:10.1029/97RS00664, 1997.

Abdu, M. A.: Outstanding problems in the equatorial ionosphere-thermosphere electrodynamics relevant to spread F, J. Atmos. Solar-Terrestrial Phys., 63(9), 869–884, doi:10.1016/S1364-6826(00)00201-7, 2001.

Abdu, M. A.: Electrodynamics of ionospheric weather over low latitudes, Geosci. Lett., 3(1), 11, doi:10.1186/s40562-016-0043-6, 2016.

Abdu, M. A., Bittencourt, J. A. and Batista, I. S.: Magnetic declination control of the equatorial F region dybamo electric field development and spread F, Jgr, 86(A13), 1143–11446, doi:10.1029/JA086iA13p11443, 1981.

Abdu, M. A., Batista, I. S. and Sobral, J. H. A.: A New Aspect of Magnetic Declination Control of Equatorial Spread F and F Region Dynamo, J. Geophys. Res. Sp. Phys., 97(A10), 14,897-14,904, doi:10.1029/92JA00826, 1992.

Abdu, M. A., Alam Kherani, E., Batista, I. S., De Paula, E. R., Fritts, D. C. and Sobral, J. H. A.: Gravity wave initiation of equatorial spread F/plasma bubble irregularities based on observational data from the SpreadFEx campaign, Ann. Geophys., 27(7), 2607–2622, doi:10.5194/angeo-27-2607-2009, 2009.

Aveiro, H. C., Denardini, C. M. and Abdu, M. A.: Climatology of gravity waves-induced electric fields in the equatorial E region, J. Geophys. Res. Sp. Phys., 114(A11), 308, doi:10.1029/2009JA014177, 2009.

Balan, N., Liu, L. and Le, H.: A brief review of equatorial ionization anomaly and ionospheric irregularities, Earth Planet. Phys., 2(4), 257–275, doi:10.26464/epp2018025, 2018.

Basu, S., Basu, S., Aarons, J., McClure, J. P. and Cousins, M. D.: ON THE COEXISTENCE OF KILOMETER- AND METER-SCALE IRREGULARITIES IN THE NIGHTTIME EQUATORIAL F REGION., J Geophys Res, 83(A9), 4219–4226, doi:10.1029/JA083iA09p04219, 1978.

Batista, I. S., Abdu, M. A. and Bittencourt, J. A.: Equatorial F region vertical plasma drifts: Seasonal and longitudinal asymmetries in the American sector, J. Geophys. Res. Sp. Phys., 91(A11), 12055–12064, doi:10.1029/JA091iA11p12055, 1986.

Booker, H. G. and Wells, H. W.: Scattering of radio waves by the F -region of the ionosphere, J. Geophys. Res., 43(3), 249, doi:10.1029/TE043i003p00249, 1938.

Bowman, G. G.: A relationship between "spread-F" and the height of the F2 ionospheric layer, Aust. J. Phys., 13, 69–72, doi:10.1071/PH600069, 1960.

Bowman, G. G.: A review of some recent work on mid-latitude spread-F occurence as detected by ionosondes, J. Geomag. Geoelectr., 42, 109–138, 1990.

Bowman, G. G.: Short-term delays (hours) of ionospheric spread F occurrence at a range of latitudes, following geomagnetic activity, J. Geophys. Res. Atmos., doi:10.1029/98JA00630, 1998.

Candido, C. M. N., Batista, I. S., Becker-Guedes, F., Abdu, M. A., Sobral, J. H. A. and Takahashi, H.: Spread F occurrence over a southern anomaly crest location in Brazil during June solstice of solar minimum activity, J. Geophys. Res. Sp. Phys., doi:10.1029/2010JA016374, 2011.

Dabas, R. S., Singh, L., Lakshmi, D. R., Subramanyam, P., Chopra, P. and Garg, S. C.: Evolution and dynamics of equatorial plasma bubbles: Relationships to ExB drift, postsunset total electron content enhancements, and equatorial electrojet strength, Radio Sci., 38(4), 1075, doi:10.1029/2001RS002586, 2003.

Dao, T., Otsuka, Y., Shiokawa, K., Nishioka, M., Yamamoto, M., Buhari, S. M., Abdullah, M. and Husin, A.: Coordinated observations of postmidnight irregularities and thermospheric neutral winds and temperatures at low latitudes, J. Geophys. Res. Sp. Phys., doi:10.1002/2017JA024048, 2017.

Eccles, J. V., St. Maurice, J. P. and Schunk, R. W.: Mechanisms underlying the prereversal enhancement of the vertical plasma drift in the low-latitude ionosphere, J. Geophys. Res. Sp. Phys., 120(6), 4950–4970, doi:10.1002/2014JA020664, 2015.

Fejer, B. G., Scherliess, L. and de Paula, E. R.: Effects of the vertical plasma drift velocity on the generation and evolution of equatorial spread F, J. Geophys. Res. Sp. Phys., 104(A9), 19859–19869, doi:10.1029/1999JA900271, 1999.

Gentile, L. C., Burke, W. J. and Rich, F. J.: A global climatology for equatorial plasma bubbles in the topside ionosphere, Ann. Geophys., 24(1), 163–172, doi:10.5194/angeo-24-163-2006, 2006.

Haldoupis, C., Kelley, M. C., Hussey, G. C. and Shalimov, S.: Role of unstable sporadic-E layers in the generation of midlatitude spread F, J. Geophys. Res. Sp. Phys., doi:10.1029/2003JA009956, 2003.

Heelis, R. A.: Electrodynamics in the low and middle latitude ionosphere: A tutorial, J. Atmos. Solar-Terrestrial Phys., 66(10), 825–838, doi:10.1016/j.jastp.2004.01.034, 2004.

Hoang, T. L., Abdu, M. A., MacDougall, J. and Batista, I. S.: Longitudinal differences in the equatorial spread F characteristics between Vietnam and Brazil, Adv. Sp. Res., 45(3), 351–360, doi:10.1016/j.asr.2009.08.019, 2010.

Huang, C. S.: Effects of the postsunset vertical plasma drift on the generation of equatorial spread F, Prog. Earth Planet. Sci., 5(1), doi:10.1186/s40645-017-0155-4, 2018.

Jiao, Y. and Morton, Y. T.: Comparison of the effect of high-latitude and equatorial ionospheric scintillation on GPS signals during the maximum of solar cycle 24, Radio Sci., 50(9), 886–903, doi:10.1002/2015RS005719, 2015.

Kil, H. and Heelis, R. A.: Global distribution of density irregularities in the equatorial ionosphere, J. Geophys. Res. Sp. Phys., doi:10.1029/97ja02698, 1998.

Klinngam, S., Supnithi, P., Rungraengwajiake, S., Tsugawa, T., Ishii, M. and Maruyama, T.: The occurrence of equatorial spread-F at conjugate stations in Southeast Asia, Adv. Sp. Res., 55(8), 2139–2147, doi:10.1016/j.asr.2014.10.003, 2015.

Krall, J., Huba, J. D., Joyce, G. and Hei, M.: Simulation of the seeding of equatorial spread F by circular gravity waves, Geophys. Res. Lett., 40, 1–5, doi:10.1029/ 2012GL054022, 2013.

Kudeki, E. and Bhattacharyya, S.: Postsunset vortex in equatorial F -region plasma drifts and implications for bottomside spread- F, J. Geophys. Res. Sp. Phys., doi:10.1029/1998JA900111, 1999.

Lee, C. C.: Occurrence and onset conditions of postsunset equatorial spread F at Jicamarca during solar minimum and maximum, J. Geophys. Res. Sp. Phys., 115(10), 1–7, doi:10.1029/2010JA015650, 2010.

Lee, C. C., Liu, J. Y., Reinisch, B. W., Chen, W. S. and Chu, F. D.: The effects of the pre-reversal ExB drift, the EIA asymmetry, and magnetic activity on the equatorial spread F during solar maximum, Ann. Geophys., 23(3), 745–751, doi:10.5194/angeo-23-745-2005, 2005.

Li, G., Ning, B., Liu, L., Ren, Z., Lei, J. and Su, S.-Y.: The correlation of longitudinal/seasonal variations of evening equatorial pre-reversal drift and of plasma bubbles, in Annales Geophysicae, vol. 25, pp. 2571–2578., 2008.

Li, G., Otsuka, Y., Ning, B., Abdu, M. A., Yamamoto, M., Wan, W., Liu, L. and Abadi, P.: Enhanced ionospheric plasma bubble generation in more active ITCZ, Geophys. Res. Lett., (43), 2389–2395, doi:10.1002/2016GL068145, 2016.

Madhav Haridas, M. K., Manju, G. and Pant, T. K.: On the solar activity variations of nocturnal F region vertical drifts covering two solar cycles in the Indian longitude sector, J. Geophys. Res. Sp. Phys., doi:10.1002/2014JA020561, 2015.

Manju, G. and Madhav Haridas, M. K.: On the equinoctial asymmetry in the threshold height for the occurrence of equatorial spread F, J. Atmos. Solar-Terrestrial Phys., 124, 59–62, doi:10.1016/j.jastp.2015.01.008, 2015.

Manju, G., Madhav Haridas, M. K. and Aswathy, R. P.: Role of gravity wave seed perturbations in ESF day-to-day variability: A quantitative approach, Adv. Sp. Res., 57(4), 1021–1028, doi:10.1016/j.asr.2015.12.019, 2016.

415 Maruyama, T. and Matuura, N.: Longitudinal variability of annual changes in activity of equatorial spread F and plasma bubbles, J. Geophys. Res., 89(A12), 10903, doi:10.1029/JA089iA12p10903, 1984.

Maruyama, T., Saito, S., Kawamura, M. and Nozaki, K.: Thermospheric meridional winds as deduced from ionosonde chain at low and equatorial latitudes and their connection with midnight temperature maximum, J. Geophys. Res. Sp. Phys., 113(9), 1–9, doi:10.1029/2008JA013031, 2008.

420 Miller, C. A.: Electrodynamics of midlatitude spread F 2. a new theory of gravity wave electric fields, J. Geophys. Res. A Sp. Phys., doi:10.1029/96JA03840, 1997.

Narayanan, V. L., Sau, S., Gurubaran, S., Shiokawa, K., Balan, N., Emperumal, K. and Sripathi, S.: A statistical study of satellite traces and evolution of equatorial spread F, Earth, Planets Sp., 66(1), 1, doi:10.1186/s40623-014-0160-4, 2014.

Otsuka, Y.: Review of the generation mechanisms of post-midnight irregularities in the equatorial and low-latitude ionosphere, Prog. Earth
425 Planet. Sci., doi:10.1186/s40645-018-0212-7, 2018.

De Paula, E. R., Muella, M. T. A. H., Sobral, J. H. A., Abdu, M. A., Batista, I. S., Beach, T. L. and Groves, K. M.: Magnetic conjugate point observations of kilometer and hundred-meter scale irregularities and zonal drifts, J. Geophys. Res. Sp. Phys., 115(8), doi:10.1029/2010JA015383, 2010.

Pezzopane, M., Zuccheretti, E., Abadi, P., De Abreu, A. J., De Jesus, R., Fagundes, P. R., Supnithi, P., Rungraengwajiake, S., Nagatsuma,
430 T., Tsugawa, T., Cabrera, M. A. and Ezquer, R. G.: Low-latitude equinoctial spread-F occurrence at different longitude sectors under low solar activity, Ann. Geophys., 31(2), 153–162, doi:10.5194/angeo-31-153-2013, 2013.

Pietrella, M., Pezzopane, M., Fagundes, P. R., Jesus, R. De, Supnithi, P., Klinngam, S., Ezquer, R. G. and Cabrera, M. A.: Journal of Atmospheric and Solar-Terrestrial Physics Equinoctial spread-F occurrence at low latitudes in different longitude sectors under moderate and high solar activity, J. Atmos. Solar-Terrestrial Phys., 164(July), e815–e818, doi:10.1016/j.jastp.2017.07.007, 2017.

435 Qian, L., Solomon, S. C. and Kane, T. J.: Seasonal variation of thermospheric density and composition, J. Geophys. Res. Sp. Phys., 114(1), doi:10.1029/2008JA013643, 2009.

Reinisch, B. W. and I. A. Galkin: Global ionospheric radio observatory (GIRO), Earth, Planets Sp., 63, 377–381, doi:10.5047/eps2011.03.001.2011, 2011.

Sastri, J. H., Ranganath Rao, H. N., Somayajulu, V. V. and Chandra, H.: Thermospheric meridional neutral winds associated with equatorial
440 midnight temperature maximum (MTM), Geophys. Res. Lett., doi:10.1029/93GL03009, 1994.

Shi, J. K., Wang, G. J., Reinisch, B. W., Shang, S. P., Wang, X., Zherebotsov, G. and Potekhin, A.: Relationship between strong range spread F and ionospheric scintillations observed in Hainan from 2003 to 2007, J. Geophys. Res. Sp. Phys., 116(8), 1–5, doi:10.1029/2011JA016806, 2011.

Smith, J. M., Rodrigues, F. S., Fejer, B. G. and Milla, M. A.: Coherent and incoherent scatter radar study of the climatology and
445 day-to-day variability of mean F region vertical drifts and equatorial spread F, J. Geophys. Res. A Sp. Phys., 121(2), 1466–1482, doi:10.1002/2015JA021934, 2016.

Stolle, C., Lür, H. and Fejer, B. G.: Relation between the occurrence rate of ESF and the equatorial vertical plasma drift velocity at sunset derived from global observations, Ann. Geophys., 26(12), 3979–3988, doi:10.5194/angeo-26-3979-2008, 2008.

Stoneback, R. A., Heelis, R. A., Burrell, A. G., Coley, W. R., Fejer, B. G. and Pacheco, E.: Observations of quiet time vertical ion drift in the
450   equatorial ionosphere during the solar minimum period of 2009, J. Geophys. Res. Sp. Phys., doi:10.1029/2011JA016712, 2011.

Su, S.-Y., Chao, C. K. and Liu, C. H.: On monthly/seasonal/longitudinal variations of equatorial irregularity occurrences and their relationship
with the postsunset vertical drift velocities, J. Geophys. Res. Sp. Phys., 113(A5), A05307, 2008.

Su, S. Y., Chao, C. K., Liu, C. H. and Ho, H. H.: Meridional wind effect on anti-solar activity correlation of equatorial density irregularity
distribution, J. Geophys. Res. Sp. Phys., 112(10), 1–11, doi:10.1029/2007JA012261, 2007.

455 Su, S. Y., Chao, C. K. and Liu, C. H.: Cause of different local time distribution in the postsunset equatorial ionospheric irregularity occur-
rences between June and December solstices, J. Geophys. Res. Sp. Phys., 114(4), A04321, doi:10.1029/2008JA013858, 2009.

Su, S. Y., Wu, C. L. and Liu, C. H.: Correlation between the global occurrences of ionospheric irregularities and deep atmospheric convective
clouds in the intertropical convergence zone (ITCZ), Earth, Planets Sp., doi:10.1186/1880-5981-66-134, 2014.

Tsunoda, R. T.: Control of the seasonal and longitudinal occurrence of equatorial scintillations by the longitudinal gradient in integrated
460 Eregion Pedersen conductivity, JGR, 90(A1), 447–456, doi:10.1029/JA090iA01p00447, 1985.

Tsunoda, R. T.: On equatorial spread F: Establishing a seeding hypothesis, J. Geophys. Res. Sp. Phys., 115(12), A12303,
doi:10.1029/2010JA015564, 2010a.

Tsunoda, R. T.: On seeding equatorial spread F during solstices, Geophys. Res. Lett., 37, L05102, doi:10.1029/2010GL042576, 2010b.

Tsunoda, R. T., Nguyen, T. T. and Le, M. H.: Effects of tidal forcing, conductivity gradient, and active seeding on the climatology of
465 equatorial spread F over Kwajalein, J. Geophys. Res. Sp. Phys., 120(1), 632–653, doi:10.1002/2014JA020762, 2015.

Vichare, G. and Richmond, A. D.: Simulation study of the longitudinal variation of evening vertical ionospheric drifts at the magnetic equator
during equinox, J. Geophys. Res. Sp. Phys., 110(A5), 1–8, doi:10.1029/2004JA010720, 2005.

Wang, G. J., Shi, J. K., Wang, Z., Wang, X., Romanova, E., Ratovsky, K. and Polekh, N. M.: Solar cycle variation of ionospheric parameters
over the low latitude station Hainan, China, during 2002–2012 and its comparison with IRI-2012 model, Adv. Sp. Res., 60(2), 381–395,
470 doi:10.1016/j.asr.2016.12.013, 2017.

Whalen, J.A.: Dependence of equatorial bubbles and bottomside spread F on season, magnetic activity, and E? B Drift velcity during solar
maximum,J, Geophys.Res.Sp.Phys. 107(A2), doi: 10.1029/2001JA000039,2002.

Woodman, R. F. and La Hoz, C.: RADAR OBSERVATIONS OF F REGION EQUATORIAL IRREGULARITIES., J Geophys Res, 81(31),
5447–5466, doi:10.1029/JA081i031p05447, 1976.